Monte Carlo study of Si diode response in electron beams

Lilie L. W. Wang and David W. O. Rogers
Physics Department, Carleton University, Ottawa K1S 5B6, Canada

(Received 11 June 2006; revised 6 March 2007; accepted for publication 7 March 2007; published 24 April 2007)

Silicon semiconductor diodes measure almost the same depth-dose distributions in both photon and electron beams as those measured by ion chambers. A recent study in ion chamber dosimetry has suggested that the wall correction factor for a parallel-plate ion chamber in electron beams changes with depth by as much as 6%. To investigate diode detector response with respect to depth, a silicon diode model is constructed and the water/silicon dose ratio at various depths in electron beams is calculated using EGSnrc. The results indicate that, for this particular diode model, the diode response per unit water dose (or water/diode dose ratio) in both 6 and 18 MeV electron beams is flat within 2% versus depth, from near the phantom surface to the depth of R_{50} (with calculation uncertainty <0.3%). This suggests that there must be some other correction factors for ion chambers that counter-balance the large wall correction factor at depth in electron beams. In addition, the beam quality and field-size dependence of the diode model are also calculated. The results show that the water/diode dose ratio remains constant within 2% over the electron energy range from 6 to 18 MeV. The water/diode dose ratio does not depend on field size as long as the incident electron beam is broad and the electron energy is high. However, for a very small beam size (1×1 cm^2) and low electron energy (6 MeV), the water/diode dose ratio may decrease by more than 2% compared to that of a broad beam.
[DOI: 10.1118/1.2722720]

Key words: Monte Carlo simulation, silicon diode detector, electron beam, radiation dosimetry

I. INTRODUCTION

Silicon semiconductor diodes have much smaller sizes than ion chambers with the same sensitivities due to the high density of silicon (compared to air) and the low energy (~3.6 eV) needed to produce an ion pair. They have been widely employed in clinical radiotherapy practice for years: either as depth-dose and dose-profile measuring devices or as quality assurance tools for *in vivo* dosimetry.[1,2] It is well known that dosimetry diodes measure almost the same depth-dose distributions in both photon and electron beams as ion chambers.[3–11] A recent Monte Carlo study in ion chamber dosimetry has suggested that in electron beams the wall correction factor (P_{wall}) for thimble ion chambers changes with depth by 2.5%[12] and for parallel-plate ion chambers it varies by as much as 6%.[13] However, in ion chamber dosimetry it is commonly assumed that the wall correction factors are unity. Since the uncorrected ion chamber measurements agree with diode measurements, this prompts the question: does the diode response, i.e., the diode reading per unit absorbed dose to the water, change with depth in a manner similar to the ion chamber's P_{wall} correction? It is empirically assumed that the diode response is independent of depth in a phantom, but this has never been proven except by making (now apparently inaccurate) assumptions about ion chamber dosimetry. If the diode response increases with depth in the same way as P_{wall}, then the measured data would be consistent; if not, we will have to find some other explanation of why there is such good agreement given the 6% (or 2.5%) wall correction factors for ion chambers, which up to now are ignored by ion chamber-based dosimetry protocols and ignored when making comparisons to diode detectors.

For this study, we are using the EGSnrc[14,15] Monte Carlo code to model a silicon diode and study its response with respect to depth in a water phantom in electron beams. In addition, we also study the energy dependence of the response of the diode model, which is an important characteristic of any radiation detector, and the field-size dependence of the response of the diode model, which is important for output factor measurements in clinical practice. The code used in this work is CSnrc,[16] a new EGSnrc user-code that implements a correlated sampling technique. CSnrc is very efficient in calculating dose ratios for similar geometries that are commonly encountered in radiation dosimetry. It has been extensively used in ion chamber dosimetry[12,13] and can be applied to many other applications as well. As an additional verification of the code, we have used CSnrc to calculate the energy and beam quality dependence of the response of LiF TLD chips in mega-voltage photon and electron beams. The results agree within the calculation uncertainty of <1% with those calculated by Mobit *et al.*[17,18] using EGS4/PRESTA.[19,20]

II. MATERIALS AND METHODS

A. Simulation of a Si diode detector

The electric current generated by a silicon diode detector is assumed to be proportional to the energy deposited in the sensitive volume or active region of the Si crystal of the diode. The model of the Si diode detector studied in most

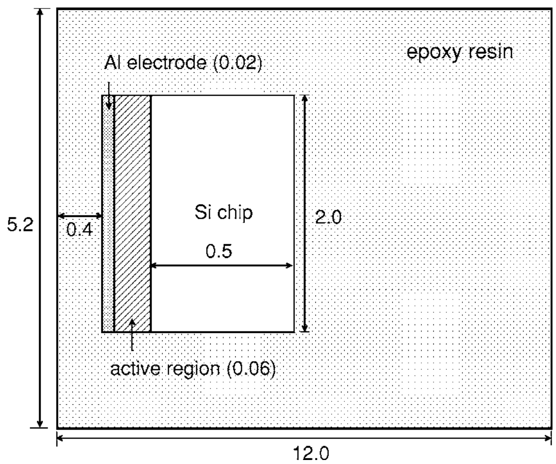

FIG. 1. Computational model 1 of a Si electron detector (not drawn to scale, dimensions in mm). Density of each material: Al, 2.70 g/cm^3; Si, 2.33 g/cm^3; epoxy resin, 1.20 g/cm^3. The constituents of epoxy resin are 76% C, 15% O, and 9% H.

detail in this work is shown in Fig. 1 and is meant to correspond to the Scanditronix-Wellhöfer EFD electron field detector. The geometrical and material data are mainly based on the information in the paper by Rikner and Grusell.[21] While this paper was under review we have obtained more detailed data from the diode manufacturer, and the model shown in Fig. 2 more accurately represents what is being sold today. Since we had done extensive computations with the first model (model 1), we present those results here for the most part. We also present some calculation results for the second model (model 2) for comparison. The active region size is the same for both the models. The major differences between the two models are (1) the overall Si chip size is larger for model 2 and the sensitive region is surrounded by a ring of Si material as the diameter of the chip size is 2.5 mm as opposed to 2.0 mm in model 1; (2) in model 2 the total Si chip thickness is 0.5 mm while in model 1 the thickness of Si behind the active region is 0.5 mm; (3) the thickness of the aluminum contact is so small (<1 μm) that it is

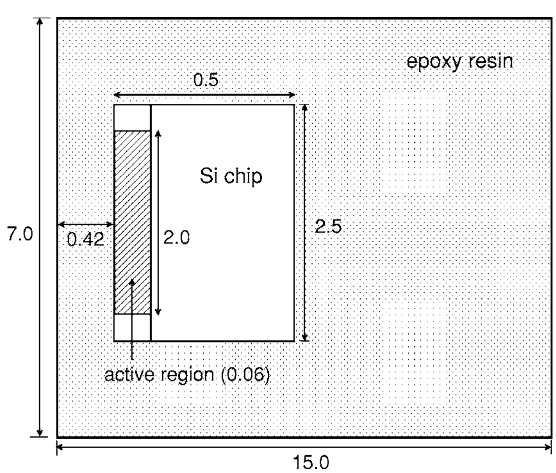

FIG. 2. Computational model 2 of the Si electron detector with the same material densities as given in Fig. 1.

removed in model 2. The diode is cylindrically shaped with the Si chip enclosed by epoxy resin. The overall size of the diode is 5.2 mm in diameter and 12 mm in length for model 1, and 7.0 mm in diameter and 15 mm in length for model 2. The active region of the Si chip is the first 0.06 mm layer of the silicon crystal. Before the Si chip there is a thin layer (0.02 mm) of aluminum for model 1. Between the aluminum and the active region, there should be a *dead layer* of silicon material, but it is so thin[22] that can be neglected completely in this study. The thickness of the dead layer for diffused junction detectors is up to about 2 μm and for other types of diode detectors it is even thinner.[22] However, Shi *et al.*[23] have reported a dead layer thickness of around 10–50 μm for some diodes used for dosimetry purposes that they have investigated, but did not have information about the type of diode we are modeling (p-type E in Shi's paper). According to the manufacturer, the thickness of the dead layer for the Scanditronix p-type EFD detector is about 3 μm. This is completely negligible in our model as is shown below where we investigate the effects of Si dead layers of 25 to 50 μm.

The modeled diode is put on the central axis of a cylindrically symmetric water phantom of radius 20 cm and depth 30 cm. The depth of the diode is determined by the depth of the center of the active region. The front face of the diode is always perpendicular to the incident direction of a parallel circular electron beam with a radius of 5.6 cm (10×10 cm^2 equivalent). The spectra of incident electron beams are from a source model of a Varian Clinac 2100C linac[24] except for the full BEAMnrc source runs described in the next section.

B. Calculation of water/silicon dose ratio and stopping-power ratio

In the Spencer-Attix formalism, the dose in a water phantom D_{water} is related to the dose in a small cavity D_{cavity} at the same location in a water phantom by

$$D_{water} = D_{cavity}\left(\frac{\bar{L}}{\rho}\right)^{water}_{cavity} P, \tag{1}$$

where $(\bar{L}/\rho)^{water}_{cavity}$ is the Spencer-Attix average restricted mass collision stopping-power ratio (SPR) of water to cavity medium and P is the product of correction factors, which is unity for an ideal cavity. For ion chambers, the cavity medium is gas and $P=P_{wall}P_{repl}P_{cel}$ is generally not unity, where P_{wall} is the wall correction factor mentioned earlier, and P_{repl} and P_{cel} are the replacement and central electrode correction factors, respectively. The size of a Spencer-Attix cavity may be characterized by a parameter Δ, which is believed to be approximately the energy of an electron that is just able to cross the cavity. For the diode model studied here, the cavity is the active region of the Si crystal. The dose D_{cavity} is the dose to silicon scored only in this active region, D_{Si}, and D_{water} is the dose to the water phantom at the same location as the Si cavity but without the presence of the diode. In addition to calculating the two dose values in one run, the water/silicon dose ratio $D_{water}/D_{\mathrm{Si}}$ is calculated directly by CSnrc.[16] This dose ratio represents the Si diode

TABLE I. Calculated d_{max}, d_{ref}, R_{50}, and R_p values for parallel incident broad electron beams of various energies. The uncertainty of d_{max} is taken as half of the width of the depth bin. The uncertainty of R_{50} is derived from the calculated dose uncertainties ($\sim$0.06%) near R_{50}.

Electron energy (MeV)	6	9	12	15	18
d_{max} (cm)	1.42±0.02	2.18±0.02	2.98±0.02	3.55±0.05	4.05±0.05
R_{50} (cm)	2.645±0.001	4.030±0.001	5.207±0.001	6.543±0.001	7.806±0.001
d_{ref} (cm)	1.487	2.318	3.024	3.826	4.584
R_p (cm)	3.3	5.0	6.3	7.8	9.4

response in a water phantom if we assume the charge released is directly proportional to the energy deposited as described in Sec. II A. In all the dose-ratio calculations, the electron and photon low-energy transport cutoffs are AE =ECUT=521 keV (i.e., the kinetic energy is 10 keV) and AP=PCUT=10 keV, respectively. For 10 keV electrons in silicon, the CSDA range is about 1.5 μm, which is negligible compared to the cavity thickness of 60 μm. Thus the cutoff of 10 keV is good enough for the calculations. For diode simulations, 5 billion histories are used to get a dose-ratio statistical uncertainty of less than 0.2% (running nearly 100 h on a single 2 GHz computer). The efficiency gain by using the correlated sampling technique to score the dose ratio averages about a factor of 3.

First, the diode is put at various depths in the water phantom and the dose ratio is calculated for both 6 and 18 MeV electron beams. Next, to study the beam quality dependence, the diode is placed at the respective reference depths for a variety of electron beams of energies ranging from 6 to 18 MeV and the dose ratio is calculated. The reference depth is $d_{ref}=0.6R_{50}-0.1$(cm) where R_{50}, the depth at which the dose falls to 50% of its maximum, and d_{max}, the depth of maximum dose, are calculated by DOSRZnrc.[25] The projected range R_p is obtained by extrapolating the maximum slope line to intercept the bremsstrahlung tail. The results are listed in Table I. The voxel sizes used in the central-axis depth-dose calculation are 1 mm in radius and 0.5 mm (for 6, 9, and 12 MeV beams) or 1 mm (for 15 and 18 MeV beams) in the depth direction. In Table I, the uncertainty on d_{max} is much larger than on R_{50} since the depth-dose curve is nearly flat near d_{max} but very steep near R_{50}, and R_{50} is derived from doses in the neighboring voxels, which can be calculated accurately.

An important issue in electron beam dosimetry is photon contamination,[26] which is fully accounted for in ion chamber dosimetry protocols such as the AAPM's TG-51.[27] However, the radiation sources we used in this study contain only electrons. To study if the photon contamination has any influence on the diode response, we implemented the capability of using a full BEAMnrc[28,29] simulation as a radiation source[30] in the CSnrc code. A BEAMnrc simulation of an Elekta SL25 linac in 22 MeV electron mode (10×10 cm^2 field size at 100 cm SSD) is compiled as a shared library and used as the radiation source for the dose-ratio calculation for the diode at different depths. A separate stand-alone simulation of the same linac by BEAMnrc is also performed and a phase space file is generated. Then, an electron beam with its spectrum extracted from the phase space file is also used as the radiation source without any photons for the dose-ratio calculation by CSnrc. The higher electron energy (22 MeV) is selected because it has a higher photon contamination level so that the influence is more pronounced.

The water/silicon dose ratio is also calculated for different incident beam sizes in both the 6 and 18 MeV electron beams. The diode is placed at the respective d_{max} for various beams sizes (see Table II). To study if the dose ratio varies with source-surface distance (SSD), a 6 MeV point source is placed at a variety of SSDs from 80 to 130 cm above the water phantom. The dose ratio is calculated with the diode located at d_{ref}. The results show that there is no SSD dependence for this diode model with a calculation uncertainty around 0.3%, thereby justifying the use of a parallel incident beam as the radiation source.

In addition to calculating the dose ratio $D_{water}/D_{\mathrm{Si}}$ for the full diode model, the dose ratios for a bare Si chip (diode without epoxy resin and aluminum) and a thin Si chip the

TABLE II. Calculated d_{max} for a variety of beam radii for 6 and 18 MeV electron beams. Also shown are the d_{max} values normalized to R_{50} for the respective broad beams.

Beam radius (cm)	0.5	1	2	3	4	⩾6
d_{max} for 6 MeV (cm)	0.60±0.02	0.98±0.02	1.38±0.02	1.42±0.02	1.42±0.02	1.42±0.02
	$0.23R_{50}$	$0.37R_{50}$	$0.52R_{50}$	$0.54R_{50}$	$0.54R_{50}$	$0.54R_{50}$
d_{max} for 18 MeV (cm)	0.80±0.05	1.55±0.05	2.45±0.05	3.25±0.05	3.65±0.05	4.05±0.05
	$0.10R_{50}$	$0.20R_{50}$	$0.31R_{50}$	$0.42R_{50}$	$0.47R_{50}$	$0.52R_{50}$

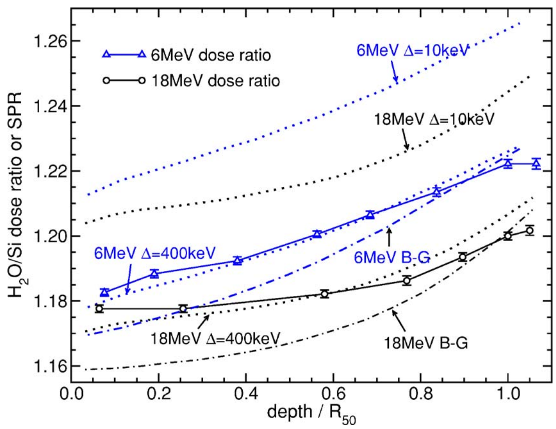

FIG. 3. Comparison of stopping power ratio calculated by SPRRZnrc with the water/silicon dose ratio calculated by CSnrc for a piece of Si with the dimensions of the active region only. Stopping powers are shown for only $\Delta=10$ keV (value used for ion chambers) and $\Delta=400$ keV, which gives the best match to the calculated dose ratios. The sources are parallel incident beams with a radius of 5.6 cm (area 100 cm^2). For the SPR curves, the error bars are not shown due to the small calculation uncertainty ($<0.02\%$).

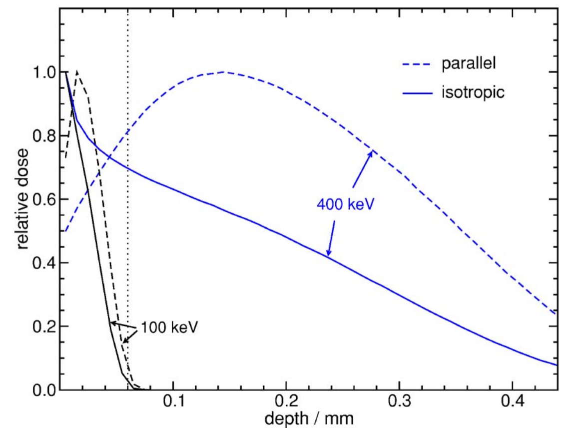

FIG. 4. Central axis depth-dose curves in Si due to parallel and isotropic source of mono-energetic, broad electron beams of energies 100 and 400 keV. Curves are calculated by DOSRZnrc with AE=10 keV. The dotted vertical line indicates the depth of 0.06 mm (the thickness of the active region of the Si crystal), which is only slightly less than the CSDA range of 100 keV electrons in Si.

size of the active region only (hereafter referred to as the ARO) are also calculated when calculating the diode response versus depth in the water phantom. Since the dose ratio is closely related to the stopping-power ratio [Eq. (1)], another EGSnrc user code, SPRRZnrc,[25] is used to calculate the water/silicon Spencer-Attix SPRs at various depths of the water phantom with the same radiation sources as used in the dose-ratio calculations. To find the Δ parameter that best characterizes the Si cavity of thickness 0.06 mm (ARO), we note that the electron energy that corresponds to a CSDA range of 0.06 mm in Si is about 85 keV. On the other hand, the mean chord length, L, calculated using the standard formula of $L=4V/S$,[31] with V the volume and S the surface area of the cavity, gives 0.1 mm, which corresponds to an energy of about 110 keV. Apparently, this energy is too small since what really matters here is the penetration depth, which could be substantially less than the CSDA range due to extensive multiple scattering. In fact, there is no definitive way to define Δ. So we investigate a variety of Δ parameters ranging from 100 to 500 keV. By comparing the results with the dose-ratio calculations as a function of depth, we can determine the most appropriate Δ parameter for the Si cavity.

III. RESULTS AND DISCUSSION

A. Thin silicon as a nearly ideal Spencer-Attix cavity

Figure 3 shows the calculated SPR and the dose ratio versus depth for the piece of Si with dimensions of the ARO in 6 and 18 MeV broad electron beams. The depth is normalized to the respective R_{50} for both beams. The four dotted lines represent the restricted SPR (or Spencer-Attix SPR) for two different values of Δ (10 and 400 keV) and for two electron beams (6 and 18 MeV). The curves for $\Delta=10$ keV, which is the value normally used in ion chamber dosimetry calculations, are included here for comparison only. The value $\Delta=400$ keV is chosen so that the Spencer-Attix SPR curves coincide as closely as possible with the corresponding dose-ratio curves near d_{max}. The two dotted dash lines, corresponding to 6 and 18 MeV beams, are Bragg-Gray SPRs calculated by a new version of SPRRZnrc.[32] The two solid lines represent the dose ratios calculated by CSnrc for the two electron beams. Although the Spencer-Attix SPR with $\Delta=400$ keV nearly converges to the Bragg-Gray SPR at R_{50}, there is about a 1% difference at the phantom surface for both of the electron beams. The curves of the dose ratio fit the Spencer-Attix SPR curves much better than the Bragg-Gray SPR curves. This indicates that the ARO behaves more like an ideal Spencer-Attix cavity, rather than a Bragg-Gray cavity, in electron beams. However, there is a small but systematic difference between the Spencer-Attix SPR and the dose-ratio curves. The discrepancy can be up to 1% at the phantom surface or at R_{50} for both electron beams. One possible cause for this 1% difference is the gradient effect in the dose build-up or fall-off area. For 6 MeV electron beams, the dose gradient at R_{50} is about 15%/mm. The thickness (0.06 mm) of the ARO is about 0.14 mm water equivalent which means the effective point of measurement is 0.04 mm deeper than the physical point of measurement, which is taken as the mid-point of the cavity. Thus the gradient correction has a magnitude of about $0.04\times 15\% \approx 0.6\%$. The gradient is in the other direction at shallow depths, consistent with the observed differences. However, this argument is not enough to explain the differences quantitatively since the gradient is smaller in the 18 MeV beam but the observed differences are larger.

To estimate the fraction of the secondary electrons that can cross the Si cavity, DOSRZnrc is used to calculate the depth-dose curves for both a parallel and an isotropic source of monoenergetic broad electron beams with energies of 100 and 400 keV. The results are shown in Fig. 4. Only a very small portion of 100 keV electrons, which have a CSDA range slightly larger than the thickness of the cavity, actually pass through the cavity, while the majority of electrons with

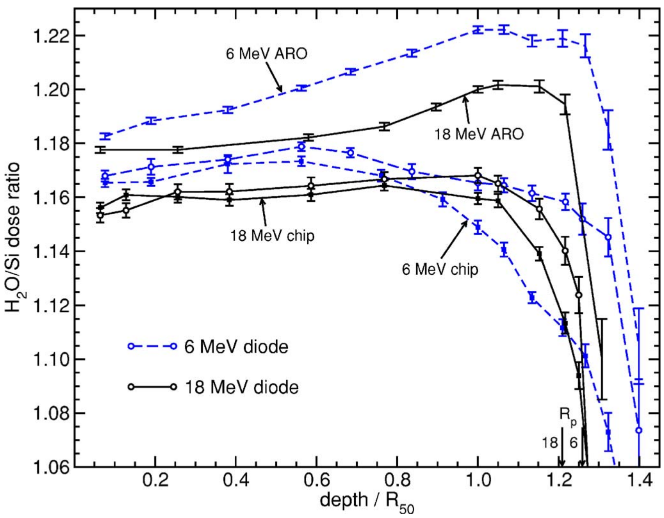

FIG. 5. The dose ratio for the Si chip and the full diode detector with respect to depth in both 6 and 18 MeV electron beams of radius 5.6 cm. Doses are scored only in the active region for both the Si chip and the diode. The depth is in units of R_{50}. R_p is indicated by an arrow on the abscissa at 1.26 for 6 MeV beam and 1.21 for 18 MeV beam.

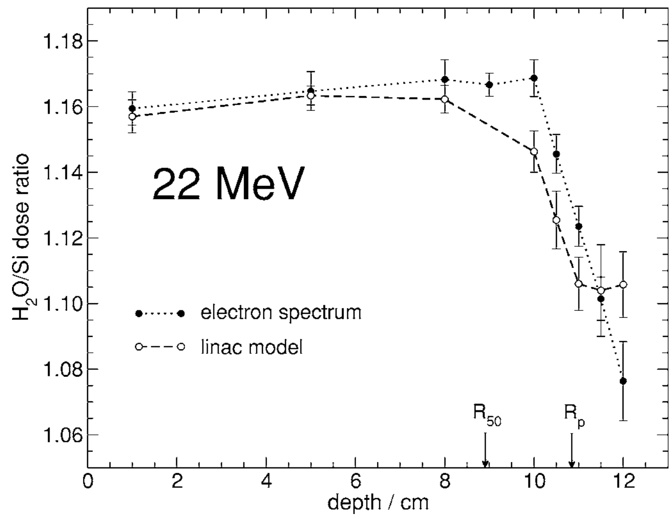

FIG. 6. The dose ratio for the diode vs. depth in a 22 MeV electron beam with field size of 100 cm^2 at 100 cm SSD. The open circles are for a BEAMnrc linac simulation as the source $(10\times 10\ \text{cm}^2)$. The solid circles are for the electron spectrum point source (5.6 cm radius). The simulated linac is an Elekta SL25 linac operating in electron mode at 22 MeV.

energy of 400 keV are able to cross the cavity for either case. Hence the standard prescription for Δ as the energy of electrons that can just cross the cavity does not appear to apply in this case. Nonetheless, the results in Fig. 3 clearly show a Δ value of about 400 keV is appropriate in this case, although $\Delta = 300$ keV is not much worse (data not shown).

B. Diode response vs. depth

The diode response is calculated as the water/silicon dose ratio for the full diode model. Unless otherwise specified, the diode model is model 1 described in Sec. II A. The calculated results for diode response versus depth for 6 and 18 MeV electron beams are shown in Fig. 5 along with the dose ratios for just the Si chip and the ARO. Several features can be observed from the figure. First, the calculated diode response is much more constant with depth compared to the ARO in both electron beams: the variation is around 2% from the phantom surface up to R_p. Next, for the Si chip in the 18 MeV electron beam, the dose ratio drops by about 4% at R_p compared with that near d_{ref}, but, in the 6 MeV electron beam, it goes down by about 7% at R_p. The dose-ratio curves for the ARO differ from all the others: they increase with depth by about 2%–4% to R_{50}, starting from a higher value as well, then remain nearly constant up to R_p. Finally, all the dose ratios drop down abruptly beyond R_p. These results show that the portion of Si crystal behind the active region plays a major role in making the diode response vs. depth flat: it supplies backscattered electrons into the active region and thus raises the dose level in the Si active region and lowers the water/silicon dose ratio, and this effect is more pronounced for lower energy beams. For the high energy (18 MeV) electron beam, the effect of the epoxy resin surrounding the Si crystal is much smaller than for the low energy(6 MeV) electron beam. The presence of the epoxy resin and aluminum cover decreases the dose in the active region, especially beyond R_{50}. If the side epoxy resin is removed, in the 6 MeV beam, the difference between the dose ratio for the full diode and for the Si chip at R_{50} is reduced to one-half and the remaining difference must be due to the epoxy and aluminum on the front surface of the Si chip. At depths beyond R_p, the dramatic drop of the water/silicon dose ratio indicates an increase in the dose to the Si cavity for the diode, the chip, and the ARO in the bremsstrahlung tail where photons dominate. This is confirmed by an independent calculation of the diode response in a Co-60 beam at depths deeper than d_{max} where the water/silicon dose ratio is more than 10% lower than in electron beams.

Figure 6 shows a comparison of the dose ratio versus depth for the two 22 MeV electron beams as described in Sec. II B: one a realistic linac simulation source with photon contamination (open circles) and the other an electron spectrum point source without photon contamination (solid circles). It is seen that from the phantom surface to a depth near R_{50} the two dose ratios agree with each other within statistics (0.4%) and vary with depth by less than 1%. Starting at R_{50} the dose ratios of both drop about 4%–5% between R_{50} and R_p. From R_{50} to R_p, the difference between the two ratios is around 2% with calculation uncertainty of 0.8%. The calculation uncertainty becomes worse since most electrons are not able to reach this point, especially for depths beyond R_p, and it takes a very long time to do the simulation. Calculations by FLURZnrc[25] have shown that the 2% difference in the dose ratios is because the average electron energy is higher at depths beyond R_{50} for the highly contaminated beam, but the electron fluence is comparable for both cases from R_{50} to R_p, and the water/silicon stopping power ratio decreases with increasing electron energy. For depths beyond R_p, the dose ratio for the noncontaminated beam (i.e., electron spectrum source) falls below that for the contaminated one. Considering this is a highly contaminated 22 MeV elec-

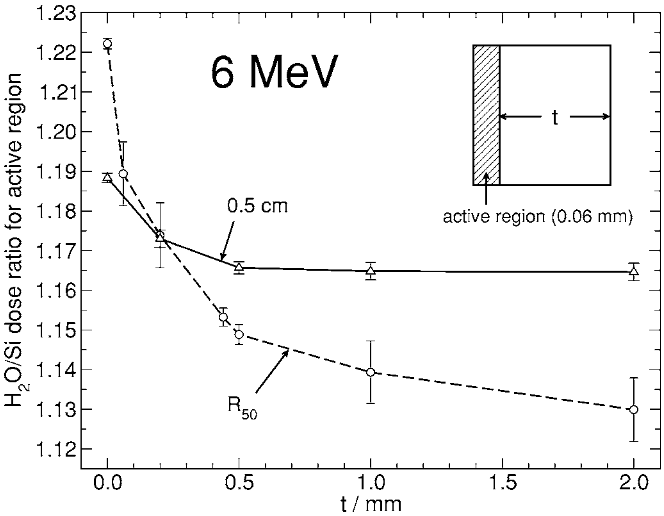

FIG. 7. Water/Si dose ratio for the active region, calculated at 0.5 cm depth and at R_{50} in a 6 MeV electron beam, vs. thickness of the Si chip. The active region has a thickness of 0.06 mm at the front of the chip.

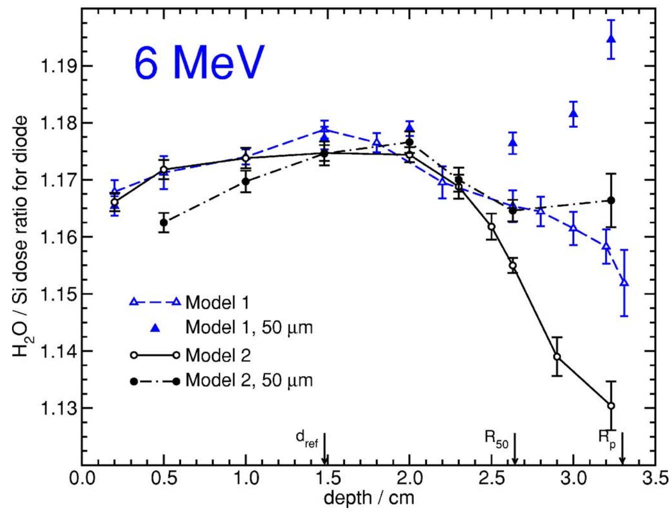

FIG. 8. Comparison of calculated water/silicon dose ratio vs. depth for model 1 (open triangle) and model 2 (open circle) diodes and the corresponding diodes with the active region displaced 50 μm below the front face of the Si chip, i.e., with a dead layer of 50 μm (solid symbol). The calculation is done in a 6 MeV electron beam.

tron beam and the difference between the two kinds of sources is only 2% up to R_p, we conclude that the difference between results for a complete beam model, which includes photon contamination and an accurate spectrum, is not significant in the cases studied in Fig. 5.

To study how the rear portion of the Si crystal contributes dose in the active region, we also calculated the water/silicon dose ratio for a Si chip of various thicknesses, with the chip located at the depth of R_{50} and at a depth of 0.5 cm, in a 6 MeV electron beam (see Fig. 7). At R_{50}, there is approximately a 7% decrease in the dose ratio when the extra Si crystal is 0.5 mm thick compared with no Si crystal at all behind the active region. On the other hand, near the phantom surface (0.5 cm depth), this difference is only about 2%. It is clear that backscatter from the silicon chip into the active region plays a significant role and increases the detector response.

As mentioned earlier, model 2 is a more accurate model of the EFD diode than model 1. So we studied as well the depth-dose characteristics of the diode model 2 and the results are presented in Fig. 8, together with those of model 1 (presented earlier in Fig. 5). The dashed and solid lines are for models 1 and 2, respectively. It is seen that, up to a depth between d_{ref} and R_{50}, there is essentially no difference in the diode response between the two models. From R_{50} to R_p, there is a significant difference: the dose ratio for model 2 is lower by 1% to 3%. The removal of the aluminum contact does not account for this discrepancy as we have compared the cases with and without the 20 μm aluminum electrode for the model 2 diode and found the two dose ratios at R_{50} agree within 0.2%. The thinner total Si chip thickness for model 2 should increase the dose ratio at R_{50} by half a percent according to Fig. 7. The only possible cause of this 1%–3% difference between the two models beyond R_{50} is the rim of Si material around active region in model 2; it provides excess low energy, side-scattered electrons into the active region, thus lowering the water/silicon dose ratio. In summary, the depth-dose characteristics for the model 2 diode is worse than that of model 1: it varies by 4% from the surface to R_p. In reality, however, this 4% difference is hard to observe since the absolute dose level near R_p is very low.

Experimentally, there has been a lot of work done to compare depth-dose curves for electron beams measured by Si diodes and by ionization chambers.[3,5–9,11] The diode used in the majority of these measurements is the one modeled in this work. Most of these results are not quantitative and only showed a general agreement between the two radiation detectors under the assumption that the diode response is uniform. This is consistent with the results here, which show a more or less flat diode response per unit dose to the water. However, most ion chamber measurements were based on stopping-power ratios for mono-energetic beams that have been shown by Burns *et al.* to be wrong by up to 1% to 2%[33] and, even if using the Burns formula for the SPR vs. depth in realistic beams, there are uncertainties at the 1% level.[34] So the comparisons between the two detectors are at best good to 1% or 2%. Considering that the value of P_{wall} varies with depth by up to 6%, any experimental comparison will be more dependent on improved ion chamber dosimetry and tell us little about diode response.

C. Beam quality and field-size dependence of the diode response

Energy or beam quality dependence is an important characteristic of a radiation detector. Figure 9 shows the calculated quality dependence for the response of both model 1 and 2 diodes placed at d_{ref} in electron beams. The electron beam quality is specified by R_{50}, the depth of dose at half maximum. There is no significant difference between the two models. Although the variation of the response in the range of electron energies from 6 to 18 MeV is about 1% to 1.5% for measurements at d_{ref}, the discrepancies may be slightly

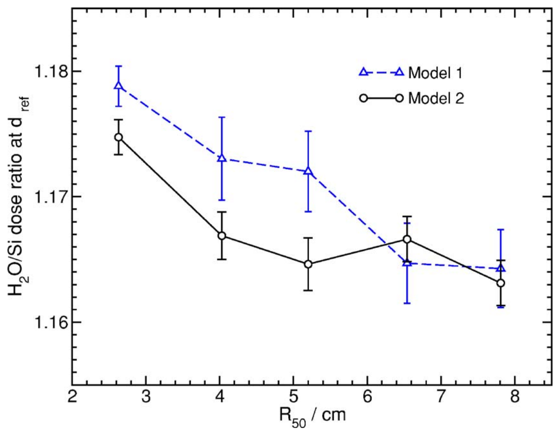

FIG. 9. Beam quality dependence of the diode's response (i.e., the dose ratio) for the two models. R_{50} is used as the beam quality specifier. The diode is placed at the reference depth d_{ref}.

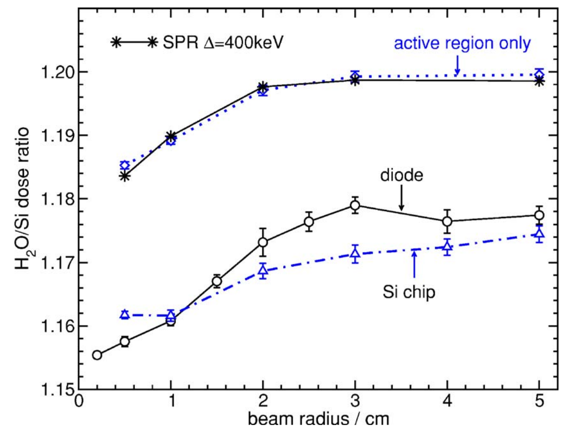

FIG. 11. Field-size dependence of the response of the diode (model 1), the Si chip, and the ARO in a 6 MeV electron beam. The diode or chip is placed at the respective d_{max} for each beam (Table II). The solid line with the star symbol is the stopping power ratio calculation with Δ=400 keV.

greater at d_{max} (see the differences in the broad beams results in Fig. 10) and overall it appears that the variation in response with energy is somewhat less than 2%.

The field-size dependence of the response of the diode model (model 1) is shown in Fig. 10. Here the field size is specified by the radius of the circularly shaped electron beam. The diode is located at the depth of maximum dose for each electron beam (Table II). For the field sizes normally used clinically (greater than 4×4 cm^2 or, in an equivalent circular beam, radius greater than 2.2 cm), the response is almost constant within the calculation uncertainty of 0.2% in both 6 and 18 MeV beams. When the field size is decreased to the radius of 0.6 cm, or 1×1 cm^2, the calculated dose ratio drops about 2% from that of the large field size in the 6 MeV beam and about 0.5% in the 18 MeV beam. For a model 2 diode, we only calculated the response for an extreme case, i.e., 6 MeV beam of radius 0.5 cm; the results for the two models agree within 0.2%. For this very small field size, we cannot compare to measurements since there are no data available experimentally, but this effect could be important in measurements when IMRT is used with electron beams.

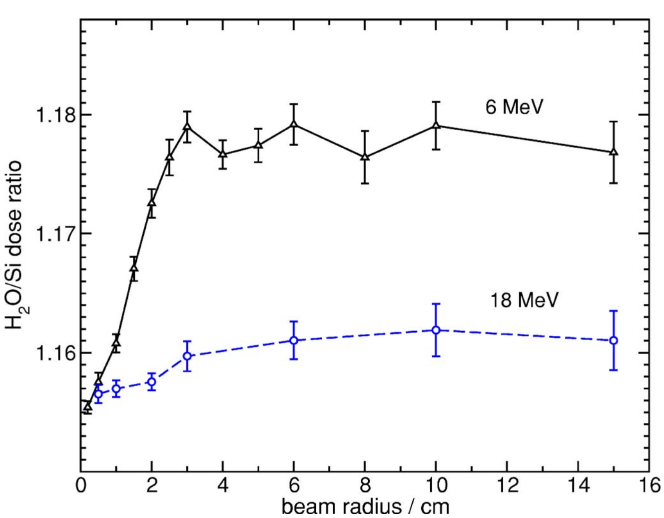

FIG. 10. Field-size dependence of the diode response in 6 and 18 MeV electron beams for the full diode model 1. The diode is placed at the respective d_{max} for each beam.

To investigate the cause of the field-size dependence of the diode response, we calculate the water/silicon dose ratio versus field size in the 6 MeV electron beam for the Si chip and the ARO. The results are shown in Fig. 11 along with the Spencer-Attix SPR calculation (Δ=400 keV) result at d_{max} (solid line with star symbol) for the respective field sizes. It is seen that both the Si chip and the ARO also exhibit the field-size dependence and the curve for the ARO almost coincides with the SPR curve, indicating that this field-size dependence comes from the SPR field-size effect that has been observed before for ion chambers.[35] This suggests that the field-size dependence is an intrinsic property of Si diode detectors in electron beams. The result also shows again, in a different perspective, that the ARO behaves like an ideal Spencer-Attix cavity in electron beams.

D. Sensitivity of the diode response on the location of the active region

For the Scanditronix EFD diode studied in this work, the active region is located at the front face of the silicon chip, i.e., the thickness of the dead layer is negligible. But some types of diode may have a significant dead layer.[23] To study how the thickness of the dead layer of the Si chip affects the diode response, we studied the cases where the active region sits below the front face of the Si chip by 25 and 50 μm, i.e., there is a 25 or 50 μm dead layer of Si before the active region, while keeping the total thickness of the Si chip fixed at 0.5 mm. The diode response is calculated at a variety of typical depths (d_{ref}, R_{50}, and R_p) in the 6 MeV electron beam for a diode of model 2 and the results are shown in Fig. 12. At R_{50}, some more data points are calculated in addition to 25 and 50 μm dead layer thicknesses in order to get a better view of the variation. At the reference depth d_{ref}, the diode response is seen not to be sensitive to the dead-layer thickness. At a deeper depth, near R_p, the response of the diode

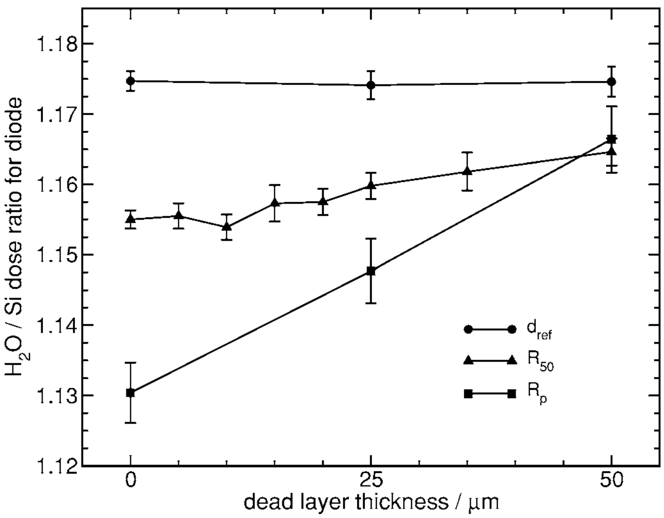

FIG. 12. Calculated water/silicon dose ratios for a diode of model 2 with different thicknesses of the dead layer. The calculation is done at three typical depths in a 6 MeV electron beam.

with 50 μm dead layer deviates from the standard one by more than 3%. This is obviously due to the attenuation of low energy electrons by the dead layer. Interestingly, this non-negligible dead layer actually makes the diode response versus depth flatter, as seen in Fig. 8. The water/silicon dose ratio is also calculated for the "50 μm dead layer" diode of model 2 in a narrow beam (0.5 cm radius) of 6 MeV electrons with the diode at d_{max}, and the result shows that the dose ratio agrees with that of the zero dead layer diode within 0.3%, indicating the field size dependence of the diode response is not sensitive to the location of the active region in the Si chip for up to 50 μm shift from the Si chip surface.

IV. CONCLUSIONS

Monte Carlo calculations of the dosimetric properties of a model of a Si diode detector in electron beams show that the diode response (i.e., dose to silicon per unit dose to water at the same point) is nearly flat with respect to depth in a water phantom, with only 2% variation up to R_{50} and about 4% variation up to R_p, in a 6 MeV beam. In isolation, the active region of the Si diode behaves almost as an ideal Spencer-Attix cavity in electron beams with an appropriately chosen Δ parameter. The selected Δ value for the Spencer-Attix SPR calculation (400 keV) is substantially higher than that normally used in ion chamber dosimetry where it is $\Delta = 10$ keV and is also considerably larger than the energy of electrons that just cross the cavity region. The portion of Si crystal behind the active region of the diode detector is the most significant factor affecting the dosimetric properties of a Si diode detector. For detectors with a relatively thick Si dead layer on the surface (25–50 μm), the dead layer will significantly influence the response at depths near R_{50} and beyond although the detector modeled here has no such dead layer. The energy independence or quality independence of the diode detector in electron beams is excellent, with less than 2% variation at d_{ref} for electron beam energies from 6 to 18 MeV. The diode response is almost independent of the field size within calculation uncertainty of 0.2% for routinely used clinical electron beams. It decreases by 2% for very small field sizes (1×1 cm^2) in low energy (6 MeV) electron beams, and the variation is partly due to the intrinsic property of the active region of the Si diode. This may prove important in IMRT with electron beams.

ACKNOWLEDGMENTS

We would like to thank Dr. Camilla Rönnqvist of Scanditronix-Wellhöfer AB for providing detailed information about the structure of the diode. We would like to thank Dr. Carl Ross at NRCC and all members of the Carleton Laboratory for Radiotherapy Physics for making useful comments on this paper. We also would like to thank Dr. N. Garry Tarr of Carleton's Department of Electronics for useful discussions about semiconductor detectors. This work is supported by the Canada Research Chair program and NSERC. The computing for this project was partially done using the CFI funded WestGrid computing resource.

[1]AAPM Task Group 62, "Diode in-vivo dosimetry for patients receiving external beam radiation therapy," Report 87, AAPM, Washington, DC, 2005.
[2]G. Leunens, J. V. Dam, A. Dutreix, and E. van der Schueren, "Quality assurance in radiotherapy by in vivo dosimetry. 1. Entrance dose measurements, a reliable procedure, Radiother. Oncol. **17**, 141–151 (1990).
[3]M. A. Trump and A. P. Pinkerton, "Application of PN junction diodes to the measurement of dose distribution of high energy radiation," Phys. Med. Biol. **12**, 573–576 (1967).
[4]L. D. Gager, A. E. Wright, and P. R. Almond, "Silicon diode detectors used in radiological physics measurements. Part I: Development of an energy compensating shield," Med. Phys. **4**, 494–498 (1977).
[5]G. Rikner, "Characteristics of a p-Si detector in high energy electron fields," Acta Radiol.: Oncol. **24**, 71–74 (1985).
[6]K. R. Shortt, C. K. Ross, A. F. Bielajew, and D. W. O. Rogers, "Electron beam dose distributions near standard inhomogeneities," Phys. Med. Biol. **31**, 235–249 (1986).
[7]R. K. Ten Haken, B. A. Fraass, and R. J. Jost, "Practical methods of electron depth-dose measurement compared to use of the NACP design chamber in water," Med. Phys. **14**, 1060–1066 (1987).
[8]P. Bjork, T. Knoos, and P. Nilsson, "Comparative dosimetry of diode and diamond detectors in electron beams for intraoperative radiation therapy," Med. Phys. **27**, 2580–2588 (2000).
[9]G. X. Ding and C. W. Yu, "Determination of percentage depth-dose curves for electron beams using different types of detectors," Med. Phys. **28**, 298–302 (2001).
[10]M. Bucciolini, F. B. Buonamici, S. Mazzocchi, C. Angelis, S. Onori, and G. A. P. Cirrone, "Diamond detector versus silicon diode and ion chamber in photon beams of different energy and field size," Med. Phys. **30**, 2149–2154 (2003).
[11]I. Griessbach, M. Lapp, J. Bohsung, G. Gademann, and D. Harder, "Dosimetric characteristics of a new unshielded silicon diode and its application in clinical photon and electron beams," Med. Phys. **32**, 3750–3754 (2005).
[12]L. A. Buckley and D. W. O. Rogers, "Wall correction factors, P_{wall}, for thimble ionization chambers," Med. Phys. **33**, 455–464 (2006).
[13]L. A. Buckley and D. W. O. Rogers, "Wall correction factors, P_{wall}, for parallel-plate ionization chambers," Med. Phys. **33**, 1788–1796 (2006).
[14]I. Kawrakow, "Accurate condensed history Monte Carlo simulation of electron transport. I. EGSnrc, the new EGS4 version," Med. Phys. **27**, 485–498 (2000).
[15]I. Kawrakow and D. W. O. Rogers, "The EGSnrc Code System: Monte Carlo simulation of electron and photon transport," Technical Report PIRS–701, National Research Council of Canada, Ottawa, Canada, 2000.

[16]L. A. Buckley, I. Kawrakow, and D. W. O. Rogers, "CSnrc: correlated sampling Monte Carlo calculations using EGSnrc," Med. Phys. **31**, 3425–3435 (2004).

[17]P. N. Mobit, A. E. Nahum, and P. Mayles, "The energy correction factor of LiF thermoluminescent dosemeters in megavoltage electron beams: Monte Carlo simulations and experiments," Phys. Med. Biol. **41**, 979–993 (1996).

[18]P. N. Mobit, P. Mayles, and A. E. Nahum, "The quality dependence of LiF TLD in megavoltage photon beams: Monte Carlo simulation and experiments," Phys. Med. Biol. **41**, 387–398 (1996).

[19]W. R. Nelson, H. Hirayama, and D. W. O. Rogers, "The EGS4 Code System, Report SLAC–265," Stanford Linear Accelerator Center, Stanford, CA, 1985.

[20]A. F. Bielajew and D. W. O. Rogers, "PRESTA: The parameter reduced electron-step transport algorithm for electron Monte Carlo transport," Nucl. Instrum. Methods Phys. Res. B **18**, 165–181 (1987).

[21]G. Rikner and E. Grusell, "Selective shielding of a p-type detector for quality independence," Acta Radiol.: Oncol. **24**, 65 (1985).

[22]G. F. Knoll, *Radiation Detection and Measurement* (Wiley, New York, 1989).

[23]J. Shi, W. E. Simon, and T. C. Zhu, "Modeling the instantaneous dose rate dependence of radiation diode detectors," Med. Phys. **30**, 2509–2519 (2003).

[24]G. X. Ding and D. W. O. Rogers, "Energy spectra, angular spread, and dose distributions of electron beams from various accelerators used in radiotherapy," National Research Council of Canada Report PIRS-0439, 1995 (see http://www.irs.inms.nrc.ca/inms/irs/papers/PIRS439/pirs439.html).

[25]D. W. O. Rogers, I. Kawrakow, J. P. Seuntjens, and B. R. B. Walters, "NRC User Codes for EGSnrc," Technical Report PIRS-702, National Research Council of Canada, Ottawa, Canada, 2000 (see http://www.irs.inms.nrc.ca/inms/irs/EGSnrc/EGSnrc.html).

[26]G. X. Ding, D. W. O. Rogers, and T. R. Mackie, "Calculation of stopping-power ratios using realistic clinical electron beams," Med. Phys. **22**, 489–501 (1995).

[27]P. R. Almond, P. J. Biggs, B. M. Coursey, W. F. Hanson, M. S. Huq, R. Nath, and D. W. O. Rogers, "AAPM's TG–51 protocol for clinical reference dosimetry of high-energy photon and electron beams," Med. Phys. **26**, 1847–1870 (1999).

[28]D. W. O. Rogers, B. A. Faddegon, G. X. Ding, C.-M. Ma, J. Wei, and T. R. Mackie, "BEAM: A Monte Carlo code to simulate radiotherapy treatment units," Med. Phys. **22**, 503–524 (1995).

[29]D. W. O. Rogers, B. Walters, and I. Kawrakow, "BEAMnrc Users Manual," NRC Report PIRS 509(a)revH (2004).

[30]I. Kawrakow and B. R. B. Walters, "Efficient photon beam dose calculations using DOSXYZnrc with BEAMnrc," Med. Phys. **33**, 3046–3056 (2006).

[31]F. H. Attix, *Introduction to Radiological Physics and Radiation Dosimetry* (Wiley, New York, 1986).

[32]T. P. Selvam and D. W. O. Rogers, "Inclusion of Bragg-Gray theory stopping-power ratios in the SPRRZnrc code," Technical Report CLRP 06-01, Carleton Laboratory for Radiotherapy Physics, Carleton University, Ottawa K1S 5B6, Canada, 2006.

[33]D. T. Burns, G. X. Ding, and D. W. O. Rogers, "R_{50} as a beam quality specifier for selecting stopping-power ratios and reference depths for electron dosimetry," Med. Phys. **23**, 383–388 (1996).

[34]D. W. O. Rogers, "Accuracy of the Burns equation for stopping-power ratio as a function of depth and R_{50}," Med. Phys. **31**, 2961–2963 (2004).

[35]G. G. Zhang, D. W. O. Rogers, J. E. Cygler, and T. R. Mackie, "Effects of changes in stopping-power ratios with field size on electron beam ROFs," Med. Phys. **25**, 1711–1724 (1998).